Mechanic-Electric-Thermal Coupling Simulation Method of Lamb Wave Under Variable Temperature

JINSONG YANG, TIANTIAN WANG and XIAOZHEN ZHANG

ABSTRACT

The propagation mechanism of Lamb waves exhibits more intricate in the variable operational environment of high-speed trains. Simulation methods are widely used to study Lamb wave propagation characteristics due to economic and time constraints. A mechanic-electric-thermal coupling simulation method to study the propagation mechanism of Lamb waves under variable temperatures is proposed in this paper. To accurately simulate the dynamic behavior of Piezoelectric Transducer (PZT) under variable temperature, a nonlinear numerical model of the dynamic parameters (piezoelectric coefficient, dielectric constant) of PZTs has been developed based on the experiment of the temperature influence on Lamb wave. The model emphasizes the nonlinear pattern of change in the key dynamic parameters of the PZT with temperature fluctuations. In addition, a thermal expansion stress model of the PZT-bonding layers-structure is established to reveal the mechanical-thermal coupling mechanism. Based on the COMSOL, a mechanical-electrical-thermal direct coupling simulation model of PZT-bonding layers- structure under variable temperature is established. The simulation results at - 40 ◦C to 80 ◦C are obtained and compared to the experiment. The results show that the simulation signal is highly consistent with the experimental measurement signal, and the simulation method proposed has high accuracy.

1. INTRODUCTION

Structural health monitoring technology identifies damage in engineering structures, providing real-time monitoring with fewer inspections and improved efficiency. Lamb wave-based methods are widely researched due to their low cost, extensive monitoring range, and sensitivity to minor damages. [1-4].

Temperature environment presents a significant challenge in developing Lamb wave-based Structural Health Monitoring (SHM)[5-8]. Lamb waves are significantly affected by temperature variations, which alter their propagation velocity, amplitude, and phase characteristics. These temperature-induced changes can mask damage features, compromising monitoring reliability. Current research focuses on mitigating these effects through baseline-free methods, environmental compensation techniques, and probabilistic modeling approaches.[9-13]. However, a large number of Lamb wave signals under time-varying conditions is required to implement these methods.

Simulation of Lamb waves under time-varying conditions offers an effective, low-cost alternative to expensive and time-consuming experiments. Finite element analysis (FEA) simulations can effectively study wave propagation in variable temperature environments while validating damage monitoring methods.[14-20]

Current research on Lamb waves in variable temperature environments primarily examines temperature effects on PZT transducers. Radecki documented significant temperature-induced changes in both velocity and amplitude of PZT-generated Lamb

Corresponding author: Jinsong Yang, E-mail address: yangjs@csu.edu.cn, School of Transportation Engineering, Central South University, No. 22 Shaoshan South Road, Tianxin District, Changsha City, Hunan Province, China, Postal Code: 410075

wave signals.[21]. Roy investigated the effect of temperature on the propagation of Lamb waves through theoretical studies and numerical analyses[22]. Research shows temperature-induced changes in Lamb wave velocity and amplitude primarily result from alterations in structural material and piezoelectric properties (piezoelectric constant and dielectric coefficient). Esfarjani's ABAQUS study across -200°C to 204°C confirmed temperature variation significantly affects Lamb wave propagation[23]. Attarian[24] using an experimental study, showed that thermal cycling reduces the sensitivity of the damage diagnosis, mainly because the nature of the adhesive layer has been altered and how the effect of the adhesive layer is not to be be ignored. In order to completely simulate the effect of temperature on Lamb wave, Lonkar[25] investigated a piezoelectric model for the propagation of Lamb wave containing an adhesive layer, where the piezoelectric and dielectric constants of PZT and the shear modulus, Poisson's ratio, and elastic modulus of the adhesive layer were modeled as a function of temperature in a simulation model. Palazotto[26] developed a 2D simulation model that contains a piezoelectric sheet 2D simulation model and investigated the effect of temperature on Lamb wave on aluminum plates using ABAQUS simulation software. The effect of temperature on the elastic modulus and Poisson's ratio of the aluminum plate was considered in the simulation model. The results show that the laser wave propagation velocity decreases as the temperature increases. Yule performed a two-dimensional guided wave simulation based on COMSOL Multiphysics software, which considered the effect of temperature on the material parameters, and obtained the law of temperature effect on Lamb wave[27]. However, these studies neglected the effect of the inconsistency of thermal expansion coefficients between different materials caused by thermal stress on the propagation of Lamb wave. The piezoelectric constants of PZT are very sensitive to thermal stress. Thermal stresses lead to changes in the piezoelectric constant of PZT, which affects the propagation of Lamb wave. Therefore, thermal stresses need to be considered.

2. SIMULATION MECHANISM OF LAMB WAVE UNDER VARIABLE TEMPERATURE ENVIRONMENT

2.1 EXCITATION-PROPAGATION-SENSING EXCITATION MODEL FOR LAMB WAVES

When PZT is used as the excitation element, the principle of generating Lamb waves through PZT excitation is the inverse piezoelectric effect. The piezoelectric constitutive formula as shown formula (1)：

$$\begin{cases} D = d\sigma + \varepsilon E \\ e = d^T E + s\sigma \end{cases} \tag{1}$$

where D is the potential shift vector (the number of charges generated per unit area on the surface of the piezoelectric element). d is the matrix of piezoelectric constants; σ is the vector of stresses; ε is the matrix of dielectric constants; E is the vector of electric fields; e is the vector of strains; and s is the matrix of elastic flexibility.

A circular PZT with $d_{31} = d_{32}$ is used to excite Lamb waves by applying voltage excitation signals in three directions. The driving strain along the x-direction at the bottom of the excitation sensor is represented by the following formula (2)：

$$\varepsilon_{act}(t) = -\frac{d_{31} V_{\text{in}}(t)}{h_{act}} \tag{2}$$

where Vin is the excitation voltage.

Based on the shear lag model, the stress generated by the PZT coupling to the structure through the adhesive layer is shown in formula (3):

$$\tau(x) = -\frac{G_{bond}}{h_{bond}} \times \frac{l_{act}\varepsilon_{act}}{\Gamma \cosh(\Gamma)} \sinh\left(\Gamma \frac{2x}{l_{act}}\right) \tag{3}$$

Where Γ is the shear lag parameter, and its expression is as follows:

$$\Gamma^2 = \frac{G_{\text{bond}}\, l_{\text{act}}^2}{h_{\text{bond}}}\left(\frac{1}{Y_{\text{act}}\, h_{\text{act}}} + \frac{\alpha}{Y_{\text{plate}}\, h_{\text{plate}}}\right) \tag{4}$$

α is a parameter that characterizes different modes.

The expressions (5) and (6) for longitudinal and transverse wave speeds are given below:

$$c_L = \sqrt{\frac{Y_{\text{plate}}\left(1-v_{\text{plate}}\right)}{\rho_{\text{plate}}\left(1+v_{\text{plate}}\right)\left(1-2v_{\text{plate}}\right)}} \tag{5}$$

$$c_T = \sqrt{\frac{Y_{\text{plate}}}{2\rho_{\text{plate}}\left(1+v_{\text{plate}}\right)}} \tag{6}$$

where v_{plate} is the Poisson's ratio of the plate and ρ_{plate} is the density of the plate.

Assuming that Lamb wave has no loss during propagation, the strain at the sensor is obtained based on the basic formula of the adhesive shear lag model. According to the positive piezoelectric effect, the voltage output is obtained as shown in formula (7):

$$V_{\text{out}}(t) = d_{31}^{\text{act}}\, C_{\text{act}}(\Gamma) C_{\text{sen}}(\Gamma)\left[\frac{d_{31}}{e_{33}s_{13}\left(1-v_{\text{act}}\right)}\right]_{\text{sen}} V_{\text{in}}(t) \tag{7}$$

where d_{31} is the piezoelectric constant of the PZT, e_{33} is the dielectric constant of the PZT, s_{33} is the elasticity coefficient of the PZT, v_{act} is the Poisson's ratio of the PZT, and *C(Γ)* is a function of the shear hysteresis parameter Γ as shown in Formulas (8) and (9):

$$C_{act}(\Gamma) = \frac{G_{\text{bond}}\left(1+v_{\text{act}}\right)R}{h_{\text{bond}}\left[(\Gamma\text{R})I_0(\Gamma\text{R}) - \left(1-v_{\text{act}}\right)I_1(\Gamma\text{R})\right]} \tag{8}$$

$$C_{sen}(\Gamma) = \frac{\iint\left(\varepsilon_{rr}^{sen} + \varepsilon_{\theta\theta}^{sen}\right) r dr d\theta\Big|_{\tau=1}}{\pi R^2} \tag{9}$$

where R is the radius of the PZT and I(ΓR) is the Bessel function.

2.2 MATERIAL PARAMETER MODEL UNDER TEMPERATURE EFFECT

Temperature impacts various materials differently: in 6061 aluminum alloy, higher temperatures decrease wave velocities, reduce elastic modulus, and increase Poisson's ratio linearly. For bonding layers, temperature primarily affects shear modulus, with typical epoxy adhesives operating between -55-100°C, while their dielectric and piezoelectric constants increase linearly with temperature, as modeled for PZT-5A in the -40~80°C range.

$$\text{P(T)} = \text{P}\left(\text{T}_0\right) + \frac{\partial \text{P(T)}}{\partial \text{T}}\Delta\text{T} \tag{10}$$

In the formula, P represents mechanical properties (Young's modulus E, Poisson's ratio v, shear modulus G, bulk modulus K), T is temperature, T_0 is ambient temperature (20°C), and ∂P(T)/∂T indicates temperature sensitivity. Sandia National Laboratory's laser ultrasound measurements of 6061 aluminum showed elastic modulus decreases linearly while Poisson's ratio increases linearly with temperature, as expressed in formulas (11) and (12).

$$E_{\text{plate}}(\Delta T) = 73.5 - 0.06 \times \Delta T \tag{11}$$

$$v(\Delta T) = 0.344 + 5.13\times10^{-5} \times \Delta T \quad (12)$$

$$G_{\text{bond}}(\Delta T) = 3.61 - 0.01\times \Delta T \quad (13)$$

Unlike metals, piezoelectric materials possess both mechanical and electrical properties, creating complex temperature dependencies. NASA's research showed PZT-5A maintains constant impedance, coupling coefficient, and dielectric loss between -55~100°C, while dielectric and piezoelectric constants increase linearly with temperature. Experiments addressing inadequate modeling yielded temperature-dependent fitting models for these constants in variable thermal environments.

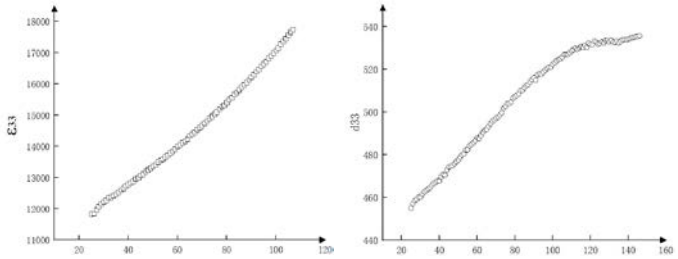

Fig. 1 Piezoelectric coefficient measurement system in variable temperature environment

A numerical model for the piezoelectric and dielectric constants of PZT-5A in the temperature range of -40◦C ~ 80◦C was investigated, as shown in formula (14) and (15). This numerical model was used for numerical simulations, but thermal stress effects were not considered.

$$d_{31}(\Delta T) = -167.7 - 0.194\times \Delta T \quad (14)$$

$$\varepsilon_{33}(\Delta T) = 2155 + 4.12\times \Delta T \quad (15)$$

Qiu studied how static loading affects Lamb wave amplitude and velocity, noting that acoustic elasticity effects cause load-dependent propagation speed changes and nonlinear stress-strain relationships. Thermal stress alters piezoelectric transducer properties by changing PZT's piezoelectric constants and dielectric coefficients, affecting wave amplitude. Formula (16) models the nonlinear relationship between load (σ in MPa) and piezoelectric constant.

$$d_{31}(\Delta\sigma) = d_{31} + d_{31}\times\left(-1.1\times10^{-5}\times\Delta\sigma^2 + 4.2\times10^{-3}\times\Delta\sigma\right) \quad (16)$$

$$d_{31}\left(\Delta T, \Delta\sigma_T\right) = -167.7 - 0.194\times\Delta T - 167.7\times\left(-1.1\times10^{-5}\times\Delta\sigma_T^2 + 4.2\times10^{-3}\times\Delta\sigma_T\right) \quad (17)$$

where ΔT is 20◦ C with respect to the reference temperature at ◦ C and $\Delta\sigma_T$ is the thermal stress in MPa.

3. SIMULATION METHOD OF LAMB WAVE UNDER TEMPERATURE EFFECT

The 3D model comprises an aluminum plate (400mm×200mm×2mm), two symmetrically arranged PZT transducers (8mm diameter, 0.48mm thickness) spaced 200mm apart, and adhesive layers (8mm diameter, 0.08mm thickness). The excitation signal Ex is defined by amplitude A, center frequency f, propagation duration t, and number of cycles N.

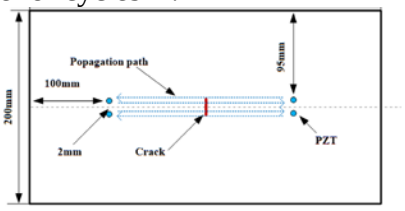

Fig. 2 Layout diagram of test specimen and sensor

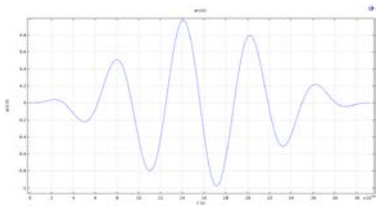

Fig. 3Excitation signal

Table 1 Material properties of aluminum plate, adhesive, and PZT

Materials	Parameters	Expression
6061 Aluminum	Elastic modulus	$E_{plate}(\Delta T)(\mathrm{GPa}) = 73.5 - 0.06\Delta T$
	Poisson's ratio	$v(\Delta T) = 0.344 + 5.13\times10^{-3}\,\Delta T$
	Density	0.33
	Coefficient of thermal expansion	2710(kg/m^3)
		2.3×10^{-5}(/k)
adhesive layer	Shear modulus	$G_{bond}(\Delta T) = 3.61 - 0.01\times\Delta T$
	Poisson's ratio	0.33
	Density	1110(kg/m^3)
	Coefficient of thermal expansion	5.4×10^{-5}(/k)
PZT	piezoelectric constant	$d_{31}(\Delta T, \Delta\sigma_T) = -167.7 - 0.194\times\Delta T$ $-167.7\times\left(-1.1\times10^{-5}\times\Delta\sigma_T^2 + 4.2\times10^{-3}\times\Delta\sigma_T\right)$
	Poisson's ratio	$e_{33}(\Delta T) = 2155 + 4.12\times\Delta T$
	Thermal Expansion Coefficient	3×10^{-6}(/k)

The simulation uses COMSOL to model Lamb wave propagation under temperature effects. Material parameters include linear elastic properties for aluminum, adhesive, and PZT, with piezoelectric properties assigned only to PZT. The model applies electric potential to one PZT's upper surface while grounding all lower surfaces, with boundary probes capturing voltage responses. For thermal stress calculation, thermal expansion is added with reference temperature T_0 and target temperature Tem, assuming uniform temperature distribution. Rigid motion suppression ensures solution convergence. Mesh sizing follows the 1/10-1/6 wavelength rule: at 200 kHz, S_0 mode (5382 m/s) and A_0 mode (1731 m/s) yield maximum mesh size <1.5mm for aluminum, with 1mm for PZT and 0.5mm for adhesive, resulting in 1.89M domain elements and 5.2M degrees of freedom.

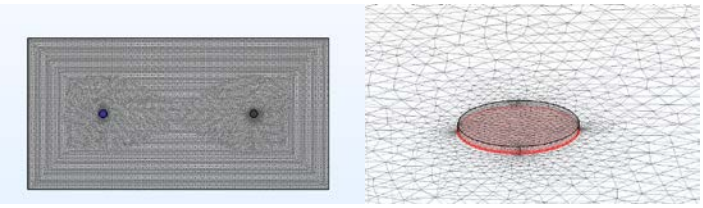

Fig. 4 Grid partitioning of PZT-adhesive layer-structure

The two-step solver simulates thermal stress and Lamb wave propagation sequentially. Step 1 uses static analysis to calculate thermal stress from differential thermal expansion, with electrostatic and piezoelectric effects disabled. These stress values are then input to parameters. Step 2 uses time-dependent analysis (0-180μs with 0.1μs steps) to simulate wave propagation, with thermal expansion and rigid motion suppression disabled. Multiple simulation runs yield Lamb wave signals across various temperature levels.

Analysis of 160kHz Lamb waves shows both S0 (faster, weaker) and A0 (slower, stronger) modes propagate normally. Temperature increases cause amplitude increases and phase delays, as demonstrated when comparing wave packets at 30μs across temperatures from -40°C to 80°C.

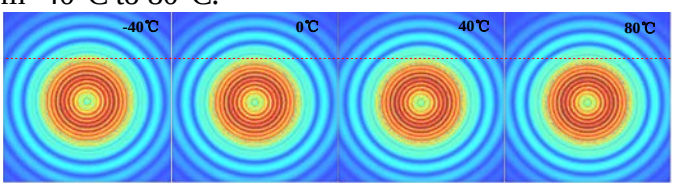

Fig.5 Effect of temperature on the phase of Lamb wave

The simulated Lamb wave signals at different temperatures are shown in Fig. 11. The magnified view of the S0 mode is given and the variation of phase and amplitude is better observed. It can be seen that the amplitude increases with time and the phase delays the increment of temperature.

4. Experimental verification of simulation methods

4.1 EXPERIMENTAL SETUP

To verify the simulation model, experiments used identical components (6061 aluminum plate 200mm×400mm×2mm, PZT 8mm×0.48mm, epoxy adhesive) with a Lamb wave SHM monitoring system and precision temperature chamber. Experimental conditions closely matched simulation parameters. Experiments covered -40°C to 80°C at 10°C intervals, with signals collected only at target temperatures during the 12-hour process. The excitation signal was a 5-cycle sine pulse modulated by ±70V Hanning window at 160kHz center frequency, sampled at 10MHz. Voltage amplification of experimental signals necessitated amplitude normalization for comparison with simulation results.

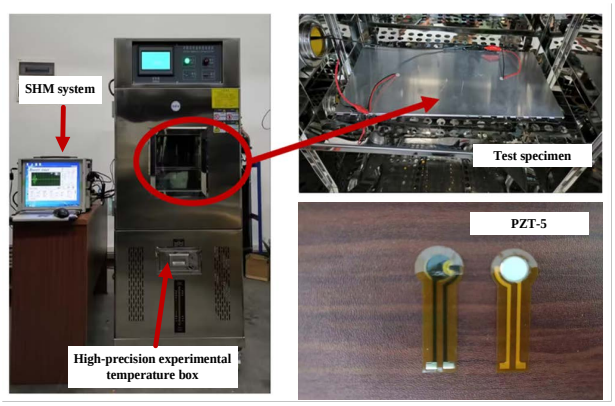

Fig. 6Overall diagram of experimental equipment

The Lamb wave signal at 160khz at different temperatures is given in Fig.13. A magnified view of the S0 mode is given, which gives a better view of the phase and amplitude variations. As the temperature increases, the amplitude increases and the phase is delayed.

4.2 COMPARISON OF SIMULATED AND EXPERIMENTAL SIGNALS

The comparison between simulated and experimental signals at temperatures of -20 ° C, 20 ° C, and 60 ° C is shown in Fig 11. The experimental signal is amplified by a charge amplifier, while the analog signal is not. Therefore, in order to better compare the simulated signal with the experimental signal, the complex continuous Shannon wavelet transform is used for filtering, and then the amplitude of S0 mode is normalized. It can be observed that the waveform matching of S0 mode is good, while the amplitude and phase errors of A0 mode are small. The reason for the error may be that the wavelength of A0 mode is smaller than S0; Therefore, the meshing size of A0 mode needs to be smaller to ensure sufficient accuracy. Measure the changes in signal amplitude and phase at different temperatures using formulas (18) and (19). Perform zero fitting on the data.

$$\Delta Amp = \frac{Amp_{Tem} - Amp_{T0}}{Amp_{T0}} \times 100\% \tag{18}$$

$$\Delta c_{\mathrm{p}} = \frac{-c_{\mathrm{p}}^2}{l_{\mathrm{p}}} \Delta t \tag{19}$$

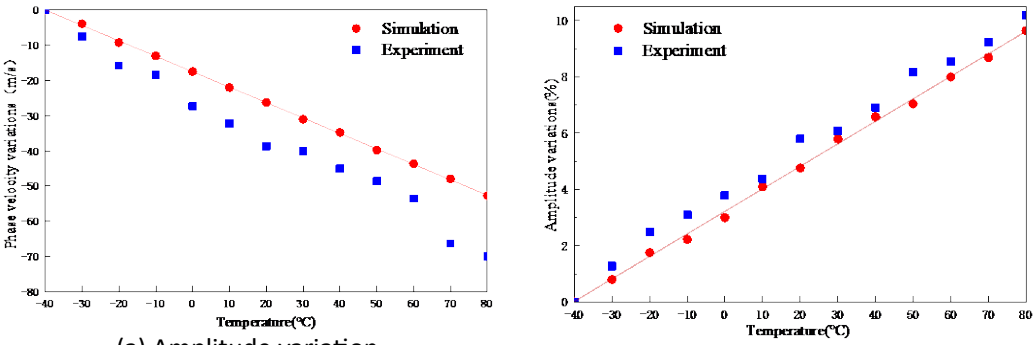

(a) Amplitude variation (b) Phase velocity change

Fig 7. Simulation and Experimental Comparison of S0 Modal Changes

Among them, Amp_{Tem} is the amplitude of the Lamb wave signal at different temperatures, Amp_{T0} is the amplitude of the Lamb wave signal at 20 ° C, cp is the phase velocity, l_p is the propagation distance of the Lamb wave, and Δt is the constant phase time shift of the Lamb wave signal. Fig 15 shows the quantitative changes in S0 modal amplitude and phase velocity between simulation and experiment. It can be seen that as the temperature increases, the amplitude increases and the phase velocity decreases. However, there may be differences in the effect of temperature on material parameters between simulation and experiment, resulting in the amplitude change rate of the experiment being greater than that of the simulation. The simulation results are in good agreement with the experimental results.

5.CONCLUSION

The numerical simulation of temperature effects on PZT-based Lamb waves shows temperature influences wave propagation through both material parameter changes and thermal stress effects on piezoelectric constants. Comparison of simulation (-40°C to 80°C) with experimental results confirms good S0 mode matching and minimal A0 mode errors. Both simulation and experiment demonstrate consistent temperature effects: increasing temperature causes amplitude increase and phase velocity decrease, though experimental amplitude changes exceed simulated rates.

REFERENCES

1. Zhou K, Zheng YB, Wu ZJ, et al. A reconstruction-based mode separation method of Lamb wave for damage detection in plate structures[J]. Smart Materials and Structures,2019,28 (3):035033.
2. Zhou DT, Huo LS, Song GB, et al. A feasibility study on monitoring of weld fatigue crack growth based on coda wave interferometry (CWI) [J]. Smart Materials and Structures,2021, 30 (9):095013.
3. Liu X, Yu Y, Li J, et al. Leaky Lamb wave–based resin impregnation monitoring with noninvasive and integrated piezoelectric sensor network[J]. Measurement, 2022, 189: 110480.
4. Wang B, Shi W, Zhao B, et al. A Modal Decomposition Imaging Algorithm for Ultrasonic Detection of Delamination Defects in Carbon Fiber Composite Plates Using Air-Coupled Lamb Wave[J]. Measurement, 2022.
5. Hu Sun, Junyan Yi, Yu Xu, et al. Identification and Compensation Technique of Non-Uniform Temperature Field for Lamb Wave-and Multiple Sensors-Based Damage Detection[J], Sensors,2019, 19(13):2930.
6. Rahim Gorgin, Ying Luo, Zhanjun Wu. Environmental and operational conditions effects on Lamb wave based structural health monitoring systems: A review[J], Ultrasonics, 2020, 105:106114.
7. Y Lu, J E Michaels. Feature extraction and sensor fusion for ultrasonic structural health monitoring under changing environmental conditions[J]. IEEE Sensors Journal, 2009,

9(11):1462-1471.
8. H Sohn. Statistical damage classification under changing environmental and operational conditions[J]. Journal of Intelligent Material Systems and Structures,2002,13(9): 561-574.
9. Su, Z Q, Zhou, C, Hong, M, Cheng, L, Wang, Q, Qing, X.L. Acousto-ultrasonics-based fatigue damage characterization: Linear versus nonlinear signal features. Mech. Syst. Signal Process. 2014, 45, 225–239.
10. Qiu L, Fang F, Yuan, SF. Improved density peak clustering-based adaptive Gaussian mixture model for damage monitoring in aircraft structures under time-varying conditions. Mech. Syst. Signal Process. 2019, 126, 281–304.
11. Ren, Y.Q, Qiu, L, Yuan, S.F, Fang, F. Gaussian mixture model and delay-and-sum based 4D imaging of damage in aircraft composite structures under time-varying conditions. Mech. Syst. Signal Process. 2020, 135, 106390.
12. Singh P, Keyvanlou M, Sadhu, A. An improved time-varying empirical mode decomposition for structural condition assessment using limited sensors. Eng. Struct. 2021, 232, 111882.
13. Qiu, L, Yuan, S.F, Chang, F.K, Bao, Q, Mei, H.F. On-line updating Gaussian mixture model for aircraft wing spar damage evaluation under time-varying boundary condition. Smart Mater. Struct. 2014, 23, 125001.
14. Shen, YF, Giurgiutiu, V. Effective non-reflective boundary for Lamb waves: Theory, finite element implementation, and applications. Wave Motion 2015, 58, 22–41.
15. Ge, L.Y, Wang, X.W, Wang, F. Accurate modeling of PZT-induced Lamb wave propagation in structures by using a novel spectral finite element method. Smart Mater. Struct. 2014, 23, 95018.
16. Hafezi, M.H, Alebrahim R, Kundu T. Peri-ultrasound for modeling linear and nonlinear ultrasonic response. Ultrasonics 2017, 80, 47–57.
17. Radecki, R, Su, Z.Q, Cheng, L, Packo, P, Staszewski, W.J. Modelling nonlinearity of guided ultrasonic waves in fatigued materials using a nonlinear local interaction simulation approach and a spring model. Ultrasonics 2018, 84, 272–289.
18. Shen YF, Giurgiutiu V. Combined analytical FEM approach for efficient simulation of Lamb wave damage detection. Ultrasonics 2016, 69, 116–228.
19. Gravenkamp H, Prager J, Saputra. The simulation of Lamb waves in a cracked plate using the scaled boundary finite element method. J. Acoust. Soc. Am. 2012, 132, 1358–1367.
20. Kumar A, Kapuria S. Finite element simulation of axisymmetric elastic and electroelastic wave propagation using local-domain wave packet enrichment. J. Vib. Acoust. 2022, 144, 021011.
21. Radecki, R, Staszewski, W.J, Uhl, T. Impact of changing temperature on Lamb wave propagation for damage detection. Key Eng. Mater. 2014, 588, 140–148.
22. Roy S, Lonkar K, Janapati V, Chang, F.K. A novel physics-based temperature compensation model for structural health monitoring using ultrasonic guided waves. Struct. Health Monit. 2014, 13, 321–342.
23. Esfarjani, S.M. Evaluation of effect changing temperature on lamb-wave based structural health monitoring. J. Mech. Energy Eng.2020, 3, 329–336.
24. Attarian, V.A, Cegla, F.B, Cawley, P. Long-term stability of guided wave structural health monitoring using distributed adhesively bonded piezoelectric transducers. Struct. Health Monit. 2014, 13, 265–280.
25. Lonkar KP. Modeling of Piezo-Induced Ultrasonic Wave Propagation for Structural Health Monitoring. Ph.D. Thesis, Stanford University, Palo Alto, CA, USA, 2013.
26. Han SJ, Palazotto AN Leakeas. Finite-element analysis of Lamb wave propagation in a thin aluminum plate. J. Aerospace Eng. 2018, 22, 185–197.
27. Yule, L, Zaghari, B, Harris, N, Hill, M. Modelling and validation of a guided acoustic wave temperature monitoring system. Sensors, 2021, 21, 7390.
28. Lee HJ, Saravanos, DA. The Effect of Temperature Dependent Material Nonlinearities on the Response of Piezoelectric Composite Plates, NASA Technical Memorandum, NASA: Brook Park, OH, USA, 1997, pp. 1–20.
29. Qiu L, Lin XD, Yuan SF. Multiphysics simulation method of lamb wave propagation with piezoelectric transducers under load condition. Chin. J. Aeronaut. 2019, 32, 1071–1086.